Transition from static to kinetic friction: insights from a 2D model

Jørgen Trømborg, Julien Scheibert, David Skålid Amundsen, Kjetil Thøgersen, Anders Malthe-Sørenssen

Transition from static to kinetic friction: insights from a 2D model

J. Trømborg,[1] J. Scheibert,[1,2] D. S. Amundsen,[1] K. Thøgersen,[1] and A. Malthe-Sørenssen[1]

[1] *Physics of Geological Processes, University of Oslo, P.O. Box 1048 Blindern, 0316 Oslo, Norway*
[2] *Laboratoire de Tribologie et Dynamique des Systèmes, CNRS, Ecole Centrale de Lyon, Ecully, France*

We describe a 2D spring-block model for the transition from static to kinetic friction at an elastic slider/rigid substrate interface obeying Amontons-Coulomb friction. By using realistic boundary conditions, a number of previously unexplained experimental results on precursory micro-slip fronts are successfully reproduced. From the analysis of the interfacial stresses, we derive a prediction for the evolution of the precursor length as a function of the applied loads, as well as an approximate relationship between microscopic and macroscopic friction coefficients. We show that the stress build-up due to both elastic loading and micro-slip-related relaxations depend only weakly on the underlying shear crack propagation dynamics. Instead, the crack speed depends strongly on both the instantaneous stresses and the friction law, through a non-trivial scaling parameter.

Frictional interfaces are important in many areas of science and technology, including seismology [1], biology [2, 3] and nanomechanics [4]. Whereas a satisfactory picture of the steady sliding regime of such interfaces has been developed during the last twenty years [5–7], the dynamics of the transition from static to kinetic friction remains elusive. During the last decade, a renewed interest has grown in such transitions, due to experimental studies that directly measured the local dynamics of frictional interfaces [8–12]. They have shown that macroscopic sliding occurs only after shear crack-like micro-slip fronts have spanned the entire contact interface.

Experimentally, micro-slip front nucleation, propagation and arrest was shown to be controlled by the instantaneous stress field at the interface. Fronts nucleate preferentially at the trailing edge of the contact area [8, 10, 13–16], an effect explained either by the enhanced shear stress near the loading point in side-driven systems [10, 13, 15, 17] or by a friction-induced pressure asymmetry in top-driven systems [8, 18]. Fronts can arise well below the macroscopic static friction threshold and arrest before the whole contact area has ruptured [13–15]. The length and number of these *precursors* depends on the precise way in which shear [13] and normal [15] forces are applied. Moreover, precursors are associated with significant changes in the spatial distribution of the real contact area [13], a quantity related to the local interfacial pressure. Finally, the propagation speed of micro-slip fronts, which covers a wide range [8–10, 19], correlates with the local shear to normal stress ratio at nucleation [16].

Theoretically, some aspects of these observations have been studied using one-dimensional (1D) models. The conditions leading to a large range of front velocities were addressed using a 1D spring-block model with a time-dependent friction law [17]. The role of an asymmetric normal loading on the length of precursors was considered using a 1D spring-block model with Amontons-Coulomb friction and different normal forces ascribed to different blocks [15]. The dependence of the series of precursors on the friction-induced pressure asymmetry was described, for Amontons-Coulomb friction, using a quasi-static 1D model [18]. In these three studies, the normal stress distribution was assumed to be uniform [17] or linear (either fixed [15] or friction-dependent [18]).

These 1D approaches were used to simplify investigation of the shear dynamics of the interface. However, they impede quantitative comparison with experimental results since determination of the actual stress field requires solution of the elastic problem for the two bodies in contact, including their precise geometry, elastic properties and boundary conditions, not only at the frictional interface but also on all their other boundaries. Ideally, this would be done via the formidable task of solving the complete 3D dynamics of the entire experimental setup. As a first step towards this, we present a 1+1D (along + orthogonal to interface) model for the transition from static to kinetic friction of an elastic slider on a rigid substrate, in which realistic boundary conditions are used. In particular, we show that considering a vertical slice of the slider is sufficient to reproduce a series of previously unexplained experimental observations.

We employed the 2D spring-block model sketched in Fig. 1a. The slider has mass M and dimensions L, B and H in the horizontal (x), transverse and vertical (z)

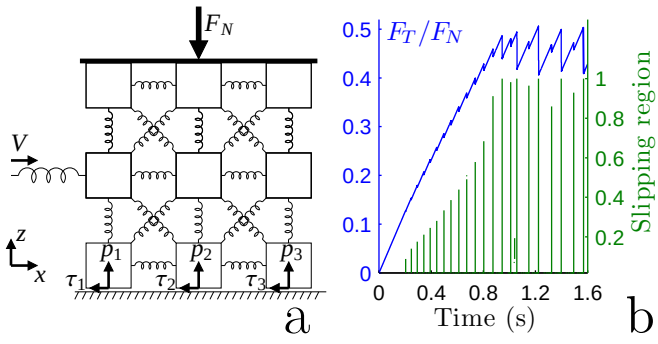

FIG. 1. (a): Sketch of the 2D spring-block model. (b) Blue: Typical loading curve, from static contact to macroscopic stick-slip, for setup 1 (h=5mm, L=140mm, F_N=3500N). Green: Locations of slipping regions for all micro-slip event. 0 (1) corresponds to the trailing (leading) edge.

directions, respectively. It is divided along a square lattice into $N = N_x N_z$ blocks of mass $m = M/N$. Blocks are coupled to their four nearest neighbours and their four next-nearest neighbours by springs of equilibrium lengths $l = L/(N_x - 1) = H/(N_z - 1)$ and $\sqrt{2}l$ and stiffnesses k and $k/2$, respectively, giving an isotropic elastic model with Young's modulus $\frac{4k}{3B}$ and Poisson's ratio 1/3. The force exerted on block i by block j is thus $k_{ij}(r_{ij} - l_{ij})\frac{\Delta \mathbf{x}_{ij}}{r_{ij}}$ when blocks are connected, 0 otherwise, where $\mathbf{x} = (x, z)$, $\Delta \mathbf{x}_{ij} = \mathbf{x}_j - \mathbf{x}_i$, $r_{ij} = |\Delta \mathbf{x}_{ij}|$ and k_{ij} and l_{ij} are the stiffness and equilibrium length of the spring connecting blocks i and j. Block oscillations are damped using a viscous force $\eta(\dot{\mathbf{x}}_j - \dot{\mathbf{x}}_i)$ on the relative motion of connected blocks. We chose the coefficient $\eta = \sqrt{0.1km}$ so that blocks are underdamped and event-triggered oscillations die out well before the next event. All η satisfying these conditions gave similar results.

Boundary conditions were designed to model two different experiments described in the literature: [13] (setup 1) and [15] (setup 2). They differ in the way the top blocks are loaded. For setup 1, they are glued to a rigid rod of mass 75.6g, itself submitted to a normal force F_N and coupled to a soft "spring mattress" of stiffness 0.4MN/m, the effect of which is modeled with a restoring torque proportional to the rod's tilt angle. For setup 2, the top blocks are submitted to a linear time-independent distribution of vertical forces $\frac{F_N}{N_x}\left(1 + \frac{2i - N_x - 1}{N_x - 1}\theta\right)$, where $\theta \in [-1, 1]$ controls the pressure asymmetry. In both setups, the bottom blocks lie on an elastic foundation of modulus $k_f = k$, i.e. each block is submitted to a vertical force of amplitude $p_i = k_f\,|z_i|$ if $z_i < 0$ or 0 otherwise, where z_i is the vertical displacement of block i. All $k_f > k$ gave similar results, so that the substrate can be considered rigid compared to the slider. Both vertical boundaries are free, except for a horizontal driving force $F_T = K(Vt - x_h)$ applied on the left-side block situated at height h above the interface, where x_h is the x-displacement of this block. This models a pushing device of stiffness K driven at a small constant velocity V. The amplitudes f_i of the friction forces on the bottom blocks follow a local Amontons-Coulomb friction law with static and kinetic friction coefficients μ_s and $\mu_k < \mu_s$. If $\dot{x}_i = 0$, f_i balances all horizontal forces on block i up to $\mu_s p_i$, at which slip initiates; then $f_i = \pm\mu_k p_i$ when $\dot{x}_i \lessgtr 0$. The $2N$ equations of motion are solved simultaneously using a fourth order Runge–Kutta integrator on a uniform temporal grid of resolution Δt.

Using this model, we simulated the transition from static to kinetic friction for the various loading configurations reported in [13] and [15]. Model parameters are given in the caption of Fig. 2. Figure 1b (blue) shows a typical loading curve for setup 1, from static contact up to macroscopic stick-slip. As in 1D models, and in agreement with experimental results, we observe, well before macroscopic sliding, a series of partial force relaxation events, corresponding to precursors, which all nucleate at the trailing edge, and extend over increasing lengths L_p (Fig. 1b, green).

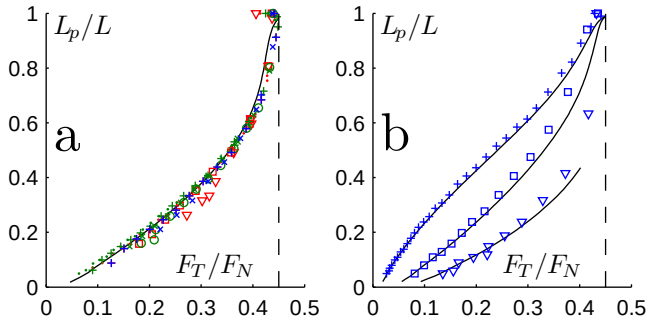

FIG. 2. Normalized precursor length L_p/L as a function of the normalized shear force F_T/F_N. (a) Setup 1 for various configurations: L=140 or 200mm, h ranges between 2.5 and 15mm, F_N=1750, 2700 or 3500N, H=75mm, B=6mm, K=4MN/m, M=75.6g, V=0.7875mm/s, l=2.5mm, k=13.5MN/m, μ_s=0.7, μ_k=0.45, Δt=0.2µs. (b) Setup 2 for θ=0.833 (+), 0 (□) or -0.833 (▽), L=100mm, H=20mm, B=5mm, K=0.8MN/m, M=12g, V=0.45mm/s, F_N=400N, h=2mm, l=1mm, k=9.375MN/m, μ_s=0.7, μ_k=0.45, Δt=0.09µs. Vertical dashes correspond to μ_k and solid lines to the prediction obtained with $\mu_s = \mu_k$ (see text).

We first focus on the dependence of L_p on the applied tangential force F_T just after relaxation. We simulated, for setup 1, different slider lengths L, pushing heights h and normal forces F_N. The behaviour under different conditions differ by the number of precursors occurring along the transition: for larger L and smaller h there are more precursors. However, Fig. 2a shows that the results for all conditions can be collapsed on a single curve by plotting L_p/L as a function of F_T/F_N. The same collapse was found in [13], with a very similar shape for the non-linear increase of L_p/L with F_T/F_N. In particular, we reproduce the transition from a roughly linear increase up to $L_p/L \sim 0.5$ to a more rapid growth for longer precursors. We emphasize that a 1D model with homogeneous normal loading would produce a purely linear increase. In Fig. 2b we compare, for setup 2, the evolutions of L_p/L as a function of F_T/F_N for three different linearly asymmetric normal loadings of the slider. Qualitatively, the lower the normal load on the trailing edge, the lower the threshold force required to nucleate precursors, and therefore the lower the tangential force F_T necessary for the precursor to reach a given length L_p, which explains the relative positions of the three curves in Fig. 2b. Again, the simulated curves are in excellent agreement with the experimental results in Fig. 8 of [15], much better than the 1D prediction (Fig. 13 of [15]). These non-trivial results for both setups clearly demonstrate that, by enabling realistic boundary conditions, 2D models do offer significantly improved agree-

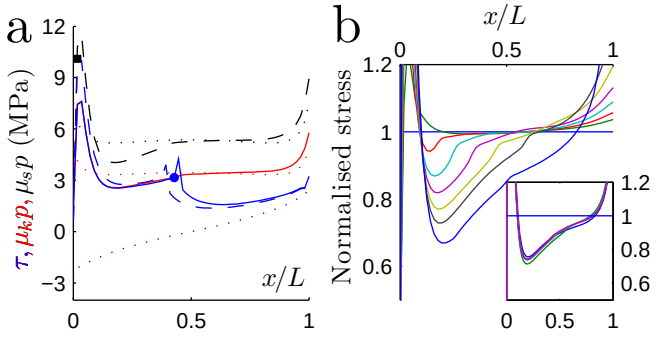

FIG. 3. (a) Spatial distribution of τ (blue), $\mu_s p$ (black) and $\mu_k p$ (red) at three stages of the transition. Dotted lines: initial configuration (F_T=0). Dashed lines: at crack initiation for the 9th precursor shown in Fig. 1b. Solid line: at crack arrest for the same precursor. Black square: nucleation point. Blue disk: arrest point. (b) Spatial distribution of p, normalized by the initial distribution, after each of the successive precursors shown in Fig. 1b. Inset: Similar distribution for system-sized events during macroscopic stick-slip.

ment with experiments.

We now use our simulation results to gain insight into how shear cracks nucleate, propagate and arrest at an interface obeying Amontons-Coulomb friction. In particular, we will examine the role played by the evolution of the shear and normal stress distributions at the interface. We emphasize that, in 2D, the latter is a result of the simulation, not an assumption, which is required in 1D. In Fig. 3a we show the typical stress evolution for setup 1. Initially ($F_T = 0$) the normal stress $p(x)$ is symmetric, with edge effects related to the flat punch geometry of the contact. The shear stress $\tau(x)$ is antisymmetric, due to friction-frustrated Poisson expansion. These stresses are in excellent agreement with those expected from contact mechanics and those measured in [16]. Application of a tangential force at the trailing edge modifies slightly the normal stress field and modifies significantly the shear stress field, with a large increase near the trailing edge over a distance of order h. The local slipping threshold $\tau(x) = \mu_s p(x)$ is therefore reached first near the trailing edge and a micro-slip front corresponding to the first precursor nucleates there. It then stops after propagation over a finite distance L_p and the whole scenario is repeated until the leading edge is reached. Figure 3a illustrates this scenario for a typical precursor event.

We find that the shear stress $\tau(x)$ just after a precursor is always very close to $\mu_k p(x)$ over the whole slipped length $x \leq L_p$. This shows that the arrest state of the interface is only weakly dependent of the static friction coefficient μ_s, and is controlled primarily by the kinetic friction coefficient μ_k. We emphasize that this behaviour is not specific to simple Amontons-Coulomb friction, but remained true for slip-weakening friction, provided the weakening distance is smaller than a few μm. Based on this behaviour, we propose the following procedure to predict, for given loading conditions and a given μ_k, the non-linear evolution of L_p with F_T (Fig. 2): We run the model for equal friction coefficients ($\mu_s = \mu_k$). The transition from static to kinetic friction in this simplified model is smooth, with a continuously growing micro-slip region within which $\tau(x) = \mu_k p(x)$. The length of the slipping region as a function of the applied force was found to be independent of the driving velocity V, and is shown in solid lines in Fig. 2. For both setups and for all loading configurations, this curve is in good quantitative agreement with the master curve for the length of precursors as a function of the arrest force. Such agreement is due to the fact that any arrest state in the full model is very similar to the state reached in the simplified model for the same force F_T. The independence of the prediction on V shows that it can be obtained using simple quasi-static calculations, i.e. it does not require a complete dynamical simulation.

The very last precursor propagated over almost the entire interface and left a shear stress that was equal almost everywhere to $\mu_k p$, yielding a total shear force $F_T \simeq \mu_k F_N$. The last increment of tangential force required to trigger the first system-sized event brings the vicinity of the trailing edge to its threshold, whereas the shear stress on the rest of the interface is essentially unchanged, yielding a maximum total shear force only slightly above $\mu_k F_N$ (see Fig. 1b). This maximum force is classically interpreted as $\mu_s^{\text{macro}} F_N$ with μ_s^{macro} the macroscopic static friction coefficient. Therefore our results suggest that, in side driven systems, whatever the value of μ_s, $\mu_s^{\text{macro}} \simeq \mu_k$. The difference between the macro- and microscopic static friction coefficients, already discussed in recent 1D models [15, 18], provides a possible explanation for the anomalously high values of μ_s compared to μ_s^{macro} reported in [16].

Not only the shear stress τ but also the normal stress p is altered along the transition. Figure 3b shows $p(x)$, normalized by the initial distribution (at $F_T = 0$), after each of the successive precursors. The normal stress is found to be significantly decreased along the path of the precursor that just occurred, by up to 30% whereas, apart from edge effects, it is mainly unchanged in front of it. The normal stress then assumes a reproducible distribution in the macroscopic stick-slip regime (Fig. 3b, inset). Recalling that, at normally loaded rough contact interfaces, normal stress is robustly found to be locally proportional to the area of real contact, the results of Fig. 3b show very good agreement with measurements of the real area of contact reported in [13] (Fig. 4a). Direct quantitative comparison is not possible, mainly because normal stress has a constant integral (normal force F_N imposed) whereas the total real area of contact is not a conserved quantity, but typically decreases by 20% across the transition [13, 20].

Let us now focus on the propagation dynamics of the simulated frictional shear cracks. Figure 4a shows the

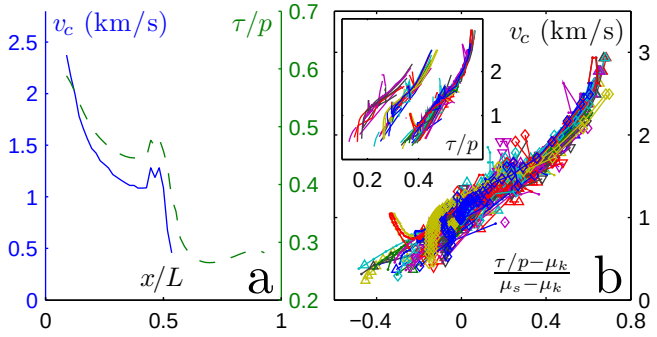

FIG. 4. (a) Local crack speed v_c (spatial average on 5 neighbouring blocks) and local shear to normal stress ratio τ/p as a function of crack length x for the 11th precursor event shown in Fig. 1b. (b) Inset: v_c as a function of τ/p. Left: run 1. Center: run 2. Right: runs 3 and 4. Main: v_c as a function of $\frac{\tau/p-\mu_k}{\mu_s-\mu_k}$. $\triangledown$: run 1. $\diamond$: run 2. $\triangle$: run 3. Dots: run 4.
Run 1: L=140mm, F_N=3500N, h=5mm, μ_s=0.5, μ_k=0.2.
Run 2: L=140mm, F_N=3500N, h=5mm, μ_s=0.55, μ_k=0.3.
Run 3: L=140mm, F_N=3500N, h=7.5mm, μ_s=0.7, μ_k=0.45.
Run 4: L=200mm, F_N=2700N, h=10mm, μ_s=0.7, μ_k=0.45.

evolution of the local crack speed v_c as a function of position x along the interface for a typical precursor event in setup 1. $v_c(x)$ decreases from around 2400m/s near the trailing edge to around 400m/s just before crack arrest and appears to be strongly correlated to the shear to normal stress ratio $\tau(x)/p(x)$. In fact, when v_c is plotted as a function of τ/p, all points corresponding to all locations x along all successive events in a given simulation collapse on a single curve (Fig. 4b, inset). Different geometries or loading conditions lead to the very same curve. Conversely, changing the values of the friction coefficients leads to different curves. All these curves can then be collapsed on the same master curve when $v_c(x)$ is plotted as a function of the non-trivial parameter $\frac{\tau(x)/p(x)-\mu_k}{\mu_s-\mu_k}$ [21], which represents the local distance to the slipping threshold. These results are a generalization, accounting for any value of the microscopic friction coefficients, of a similar collapse obtained for experimental data, from system-sized events only, using τ/p as a parameter (Fig. 3 in [16]). Our results also suggest that, if probed, precursors would follow the same experimental curve as system-sized events.

In surprising contrast with the excellent agreement found with experiments up to now, the master curve of Fig. 4b exhibits strong discrepancies with its experimental counterpart. The shape as well as the explored ranges of both v_c and τ/p are different. In particular, our model does not produce very slow micro-slip fronts like those observed in various experiments [16, 19]. Most likely this is because the simple Amontons-Coulomb friction used here lacks some time dependent ingredient necessary to yield slow fronts, like those in [17].

As a conclusion, all our results suggest two distinct levels of description of the transition from static to kinetic friction. First a *kinematic* description of (i) the slow evolution of interfacial stresses between events and (ii) the stress conditions at crack nucleation and arrest. Second, a *dynamic* description of the fast propagation of micro-slip fronts along the interface. The crack dynamics appears to depend crucially, via the friction law, on the kinematic stresses at crack initiation. Conversely, we showed that the kinematic description is essentially independent of the underlying dynamics: we could successfully reproduce all available experimental kinematic results, even with an unrealistic friction law, provided that realistic 2D boundary conditions were used.

We acknowledge funding from the European Union (Marie Curie grant PIEF-GA-2009-237089). This paper was supported by a Center of Excellence grant to PGP from the Norwegian Research Council.

[1] C. Scholz, *The Mechanics of Earthquakes and Faulting* (Cambridge University Press, 2002).
[2] M. Urbakh, J. Klafter, D. Gourdon, and J. Israelachvili, Nature **430**, 525 (2004).
[3] J. Scheibert, S. Leurent, A. Prevost, and G. Debrégeas, Science **323**, 1503 (2009).
[4] B. Bhushan, *Nanotribology and Nanomechanics* (Springer, Heidelberg, Germany, 2008).
[5] B. Persson, *Sliding Friction* (Springer, 2000).
[6] T. Baumberger and C. Caroli, Adv. Phys. **55**, 279 (2006).
[7] J. Scheibert, A. Prevost, G. Debrégeas, E. Katzav, and M. Adda-Bedia, J. Mech. Phys. Solids **57**, 1921 (2009).
[8] T. Baumberger, C. Caroli, and O. Ronsin, Phys. Rev. Lett. **88**, 075509 (2002).
[9] K. W. Xia, A. J. Rosakis, and H. Kanamori, Science **303**, 1859 (2004).
[10] S. M. Rubinstein, G. Cohen, and J. Fineberg, Nature **430**, 1005 (2004).
[11] J. Scheibert, G. Debrégeas, and A. Prevost, Arxiv:0809.3188v1 (2008).
[12] A. Chateauminois, C. Fretigny, and L. Olanier, Phys. Rev. E **81**, 026106 (2010).
[13] S. M. Rubinstein, G. Cohen, and J. Fineberg, Phys. Rev. Lett. **98**, 226103 (2007).
[14] R. Bennewitz, J. David, C. F. de Lannoy, B. Drevniok, P. Hubbard-Davis, T. Miura, and O. Trichtchenko, J. Phys.: Condens. Matter **20**, 015004 (2008).
[15] S. Maegawa, A. Suzuki, and K. Nakano, Tribol. Lett. **38**, 313 (2010).
[16] O. Ben-David, G. Cohen, and J. Fineberg, Science **330**, 211 (2010).
[17] O. Braun, I. Barel, and M. Urbakh, Phys. Rev. Lett. **103**, 194301 (2009).
[18] J. Scheibert and D. K. Dysthe, EPL **96**, 54001 (2010).
[19] S. Nielsen, J. Taddeucci, and S. Vinciguerra, Geophys. J. Int. **180**, 697 (2010).
[20] O. Ben-David, S. M. Rubinstein, and J. Fineberg, Nature **463**, 76 (2010).
[21] C. B. Muratov, Phys. Rev. E **59**, 3847 (1999).